

**Title:** CubeSat observing atmospheric and space electricity for the science of serious natural disasters: A Challenge to their mitigations  
**Primary Point of Contact (POC) & email:** Shoho Togo, f117126w@st.u-gakugei.ac.jp  
**Co-authors:** Kikuko Miyata\*, Kohei Tanaka†, Hidetoshi Nitta, Yuko Suzuki, Shusaku Takahashi, Yuto Tomita, Sumire Onagi, Akiko Ishikawa, Yusuke Ozawa†, Masashi Kamogawa  
**Organization:** Tokyo Gakugei University, \* Nagoya University, † ISAS/JAXA  
**(Yes) We apply for Student Prize.**  
**(No) Please keep our idea confidential if we are not selected as finalist/semi-finalist.**

## 1. Need

A satellite remote sensing such as optical measurements and radar monitoring have contributed to mitigating severe natural disasters. However, a large earthquake, tsunami, lightning, and global warming issue were under suffering, because their physical mechanism under the conventional remote sensing and ground-based observations was still unclear. In order to overcome the problems, we focus on atmospheric and space electricity variations – a proxy of these natural disaster occurrences – such as earthquake ionospheric precursors, tsunami ionospheric holes, thunderstorm-generated radiation, and global lightning activities. Therefore, the investigation of the atmospheric and space electricity is highly expected to reach unprecedented prediction and early warning issues. As it is possible to observe the atmospheric and space electricity by electromagnetic and optical satellite measurements, a 12U CubeSat is a feasible satellite for promoting their science.

## 2. Mission Objectives

Cube-/Nano-/Micro- satellites for earthquake (EQ) prediction have been frequently proposed in mission idea contest (MIC) and other satellite design contests. In fact, we also proposed a micro-satellite for the EQ prediction in the 2nd MIC [1]. Our proposed satellite in 4th MIC is beyond the previous idea. In other words, the following mission objectives not only includes the mission for EQ prediction but also shows various missions for contributing to significant and serious natural disaster mitigations even in a smaller satellite than the previous proposed satellite [1]. Moreover, the mission backgrounds were mainly based on our scientific papers, so that the following missions have been carefully evaluated in the scientific point of view.

### 1) Verification of earthquake ionospheric precursor for practical EQ prediction (EQ mission)

The technology of the earthquake prevention is remarkably developing and is widely used in our life, while no one can issue large earthquake occurrence in advance, because it is inconclusive whether the earthquake is predictable or not in the modern seismology. Meanwhile, a number of various earthquake precursors, especially ionospheric precursors, have been reported through various measurements, undoubtedly contributing to practical short-term earthquake prediction. Addressing a plausible ionospheric precursor observed by the satellite [1], many precursors for global large earthquakes are observable, because the lead-time, namely the duration, of the precursor are within a few hours. As a result, the ionospheric precursors are detectable because they are longer than the period of one satellite orbit. The results of plausible precursor were obtained by the French DEMETER satellite [2]. Our further statistical analysis [3] showed that VLF electric field intensity at 1.7 kHz (the earth-ionosphere waveguide cut off) decreased only near the epicenter within 4 hours before the 289  $M \geq 4.8$  EQs, using the complete DEMETER data (Fig. 1a) [3]. A plausible physical mechanism of the decrease might be caused by the electron density enhancement in D regions (Fig. 1b), which is measurable by investigating the whistler VLF electromagnetic waves in the ionosphere generated by the tropospheric lightning. Thus, the in-situ satellite measurement of the whistler waves and the ground-based lightning measurement are expected to provide the D-region variation attributed to the global EQ. In our CubeSat, we observe high-sampling VLF wave form in electric field components within 4 hours earthquake to further understand the physical mechanism of D region variation. From this study, we aim at practical EQ prediction by observing whistler waves (Fig. 1b).

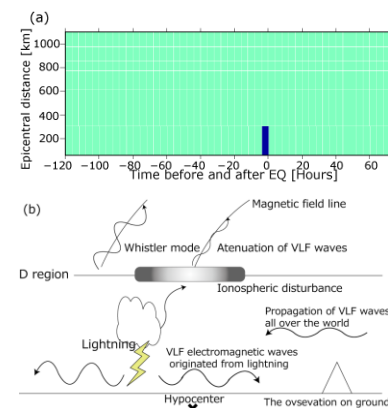


Fig. 1 (a) Averaged VLF electric field intensity in 289  $M \geq 4.8$  EQs (b) Schematic of plausible physical mechanism of pre-seismic VLF decrease.

### 2) Investigation of tsunami ionospheric hole for early warning system (Tsunami mission)

The 2004 M9.3 Sumatra EQ and the 2011 M9.0 Tohoku EQ. Most of the victims were killed by the EQ-induced tsunamis. This indicates that the present forecasting systems of tsunami height are not effective, even in Japan equipped with a dense scientific observation network. To

estimate the initial tsunami height in  $M \geq 8$  EQ from seismic data, records of long-period seismic waves for, i.e., approximately 10 min are required to compute the vertical displacement of the rupture area. As the dense network such as seismometer and ocean buoy barely exists, we are substantially in powerlessness against the large tsunami like Sumatra EQ case.

Low-frequency acoustic waves are excited by tsunamis. Acoustic wave propagation into the ionosphere disturbs the ionospheric plasma. The plasma disturbance can be detected by measurement of the total electron content (TEC) between a Global Positioning System (GPS) satellite and its ground-based receivers. From this observation we discovered a TEC depression lasting for a few minutes to tens of minutes, termed a tsunami ionospheric hole (TIH), which is formed above the tsunami source area (Fig. 2b) [4]. The largest TEC depression appears 10 to 20 minutes after the main shock (Fig. 2a). According to our paper [5], we showed the quantitative relationship between initial tsunami height and the TEC depression rate caused by a TIH, which can provide a tsunami early warning system for tsunamis that take more than 20 minutes to arrive at coastal areas with dense GPS receiving network like USA and Japan. As the ground GPS receiving stations are limited and no ionospheric vertical observation over the ocean exists, satellite ionospheric investigation on global tsunami for the early warning issue is required. In our CubeSat, a feasible GNSS occultation with collaborating other GNSS satellites such FORMOSAT3/COSMIC to further investigate TIH is conducted.

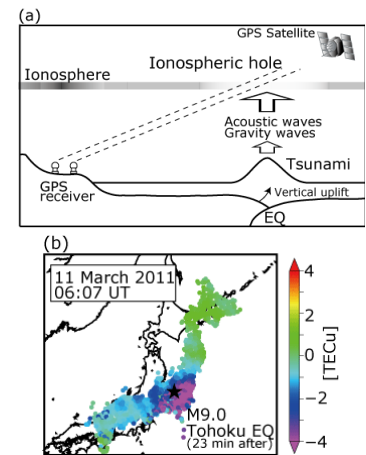


Fig.2 (a) TIH mechanism. (b) TIH on the 2011 Tohoku EQ.

### 3) Study of lightning-related phenomena for feasible lightning prediction. (Lightning mission)

Terrestrial radiation origins are uniquely known as natural radionuclide and cosmic rays discovered by several novel winners such as Marie and Pierre Curie and Victor Franz Hess. Recently, another terrestrial radiation originating from lightning was discovered initially by satellite observation for gamma-ray astronomy (terrestrial gamma-ray flashes: TGFs) [6]. Furthermore, not only lightning but also thunderstorm generates energetic radiation from recent investigations (Fig. 3a) [7]. This radiation, termed glow radiation (GR), is considered to be generated by cosmic-ray-origin electrons accelerated by thundercloud electric field [7]. As the GR ionizes atmosphere, the GR may trigger lightning (Fig. 3b), which contributes to lightning prediction through radiation measurement. Satellite altitude enables us to observe such a radiation because of low atmospheric pressure, so that epoch-making lightning prediction study can be designed by the satellite and ground-based observations of GR and lightning, respectively.

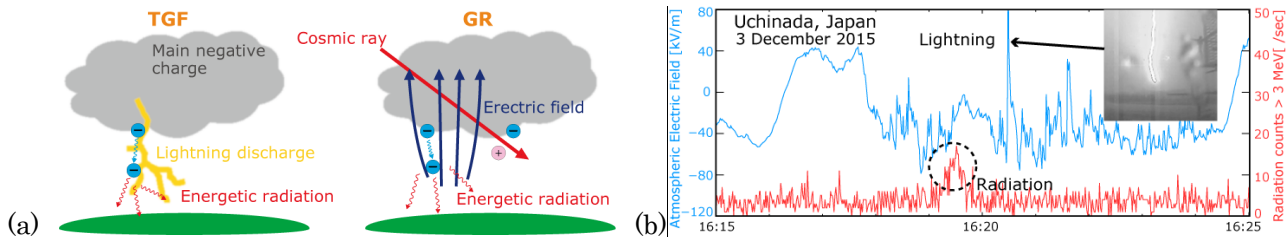
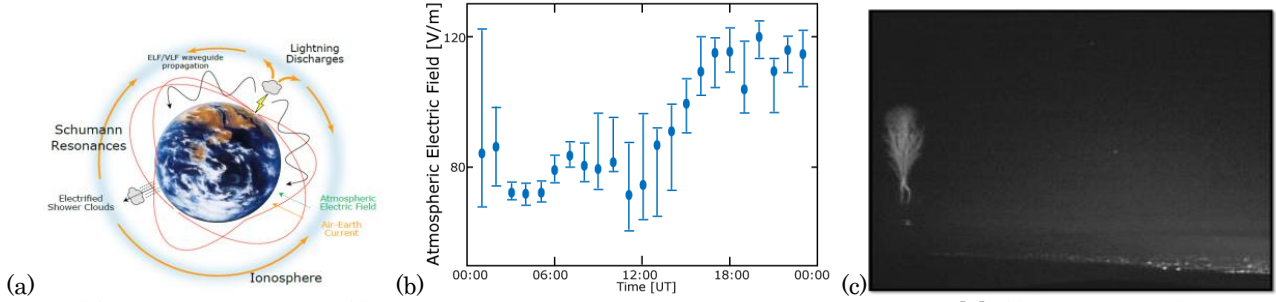


Fig. 3 (a) Schematic of TGF & GR mechanisms. (b) Pre-lightning GR was observed on the ground.

### 4) Study of global lightning for global warming understanding (Global warming mission)

On the earth, not only geomagnetic field but also vertical DC atmospheric electric field (AEF) in fair-weather (around 100 V/m near the ground) existed. The origin of AEF can be explained by the global electric circuit (GEC) conception (Fig. 4a). In GEC, cloud-to-ground (CG) lightning as well as precipitation positively and air-earth current in fair-weather region charges and discharges the ionosphere, respectively. Due to the daily variation of global CG lightning and precipitation, the AEF also varies, of which the daily variation of AEF termed Carnegie curve (CC). The CC was observed in general by research vessel because of the least atmospheric noise [8] (Fig. 4b). On the other hand, the CC was seen in the intensity of Schumann resonance (SR), the resonance of lightning-induced electromagnetic waves inside the conductive earth-ionospheric waveguide, of which the harmonics frequencies are discretely 7, 14, 21, ... Hz. In other words, the SR means AC GEC. A recent study showed that the SR intensity is highly correlated to global temperature [9], which may contribute to global warming study. In addition, recent reports showed that the SR was observable in the satellite-altitude ionosphere, leaking from the conductive earth-ionosphere waveguide [10]. As the satellite SR measurement provides noiseless different from the ground-based observation, an alternative measurement for global warming science can be launched. Furthermore, transient luminous events (TLEs), mesospheric lightning-induced luminous discharge, such as sprites and gigantic jets (Fig. 4b) is considered to

be related to GCE. In order to deeply understand the relationship between the global warming and GCE, the SR and TLEs are observed in our proposed CubeSat.



**Fig. 4** (a) Schematics of GEC. (b) CC was observed in Research vessel Hakuho-maru [7]. (c) Gigantic jet (lightning-induced discharge from thunderstorm to space) was taken from the summit of Mt. Fuji on 2014.

### 3. Concept of Operations

#### 3-1. Mission probes

**1) Electric field probe (EFP):** Vertical (geocentric) and horizontal electric field components of VLF electromagnetic waves are measured. Three probes [11] are deployed (Fig. 5). From their combinations, 1 short (yaw) and long dipoles (mostly pitch) are provided. The sensors must be out of satellite sheath, of which typical extent is around  $10 \lambda_D$ , where  $\lambda_D$  is the Debye length, root of electron temperature  $T_e$  divided by electron density  $N_e$ , e. g., a few cm and  $10 \sim 20$  cm for  $N_e > 10^4$  and  $N_e \sim \text{a few } 10^2$  at polar latitudes during nighttime and in equatorial plasma bubbles, respectively. This requires that the minimum length of boom is at least 2 m.

**2) Electron density and temperature probe (ETP):** We equipped our newly-designed Langmuir probe ( $N_e$  &  $T_e$  probe) with the middle of the extended booms (Fig. 5). Although common Langmuir probe was independently equipped with the satellite, the EFP and ETP shares one boom, which is useful for CubeSat to save space and weight. The shape of the ETP is not a general pole-type probe but a cylindrical probe between two grounded cylindrical bootstraps. Coating of the cylindrical probe is the most important issue. TiN is frequently used as popular coating. However, because TiN oxidizes in air and leads to thin TiO layers on surface that are non-conductive, high  $T_e$  is measured [12]. Therefore, carbon coating is the cheapest and easiest solution, in particular under the form of DAG 213 (Acheson) paint. The equilibrium temperature of a carbon-coated sensor and embedded electronics can be maintained in  $-10^\circ \sim +70^\circ$ . One must be cautious to avoid contamination of the coating and thrusters during launch. For monitoring neighboring plasma and satellite electrification, DC component is recorded as a house keeping (HK) data.

**3) CsI scintillator (CSI):** For terrestrial radiation observation, 2 sets of  $3'' \times 3'' \times 1''$  CsI scintillator sandwiching a Pb shielding are prepared to discriminate from galaxy and solar gamma-rays. The measured energy ranges from a few to a few tens MeV in 32 channels to discriminate from background cosmic-rays. The size, energetic range, and channel numbers were estimated from the previous papers.

**4) Optical camera (OPC):** TLEs and lightning related to the GCE are observed by space-borne monochrome camera (WATEC) satisfying identifiable resolution for TLEs and detectable frequency from the satellite altitude. The camera tilts to 30 degrees to geocentric direction and for the pitch. A video recording is 60 frames per second. To identify the TLEs, one binarizes the difference image of sequent two frames. Approximate elliptical-outline with vertical axis larger than horizontal one is regarded as a sprite or a gigantic jet. This way is probably the simplest identification of TLEs, comparing with FORMOSAT2, ISS/GLISM, and TRANIS, which is suitable for CubeSat.

**5) GNSS TEC occultation (GTO):** We employ GNSS occultation receiver developed for CubeSat [13], of which weight is 200 g.

#### 3-2. Data acquisition and transfer

Table 1 and Fig. 5 show data acquisition requirements and data transfer configuration, respectively. Measured data is recorded into 2GB SD card to maintain the whole continuous data for last 4 days. Event-trigger recording data is stored into the memory for next downlink.

#### 3-3. Launcher and Ground Station

The CubeSat is planned to be launched as a piggyback, which means no launcher requirement if a main satellite orbit is sun-synchronous. Due to the huge data downlink requirement, the satellite uses S-band transmitter with two ground stations (Japan and Norway).

Table 1. Acquisition requirements

	<i>Data acquisition requirements</i>
EFP	Original records (store two days): Sampling: 40 kHz, Resolution: 16 bit, Range: 100 dB Band-pass filter: 4 Hz- 25 kHz, VLF Survey mode: 2 s (night time) FFT: 512 points VLF Burst mode: 300 s before $M \geq 4.8$ EQ ELF Survey mode: 2 s (night time) FFT: 256 pts. for $< 128$ Hz Records: Lower 36 pts.
CSI	Energy: 32 channel, Resolution: 16 bit One TGF Event trigger: 1 s sampling
OPC	Frames: 60 / , Image size: 10 kB / Frame One TLE: 2 s sampling
ETP	2 s sampling (the whole day) 16 bit
GTO	1 s sampling (L1 and L2 records)
HK	<b>1 s sampling (e.g. 3 comp. mag. field and DC EFP)</b>

### 3-4. Operation Sequence

After the separation from the launcher, the satellite might be at tumbling mode. In the first access of the Japanese station, we perform the initial satellite checks, especially the attitude components. Then, the satellite moves to be at the rate dumping mode through the ground command until the satellite rate becomes below the threshold. After that, we deploy the booms by the ground commands. Subsequently, the mission equipment health checks are performed and the satellite shifts to the nominal mode. If the battery voltage becomes below the threshold, the satellite shut down the almost all equipment except the main computer, power controller, and command receiver.

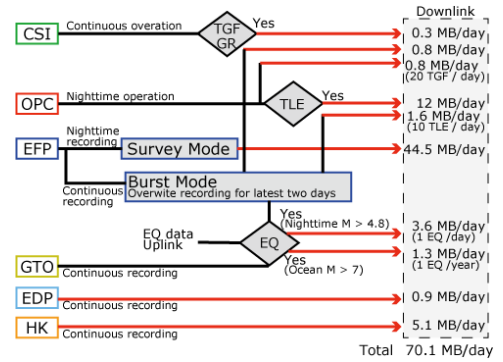


Fig. 5 Data recording and transfer

### 4. Key Performance Parameters

- 1) Lifetime of the satellite:** The expected lifetime is determined by the total required events for EQ, tsunami, and lightning (including TLEs) missions and by the total required duration for global warming mission to observe seasonable variations. Therefore, the required lifetime of the CubeSat operation is at least 2 years.
- 2) Orbit:** The key performance of the orbit is sun-synchronous orbit for statistical study of EQ mission, detectable image for lightning, and measurable SR for global warming mission.
- 3) Attitude control and determination:** An altitude control and determination is required for the EMP measurement. In order to measure the background ELF and VLF electromagnetic waves, the required control accuracy is  $< 37$  degree and determination accuracy is  $< 5$  degree. Yaw rotation must be less than one per min for a practical short dipole measurement.
- 4) Sensitivity of probes:** The probe sensitivity for 5 instruments is estimated by previous literatures including ours results of space and ground-based observations.



Fig. 6 Satellite Schematics.

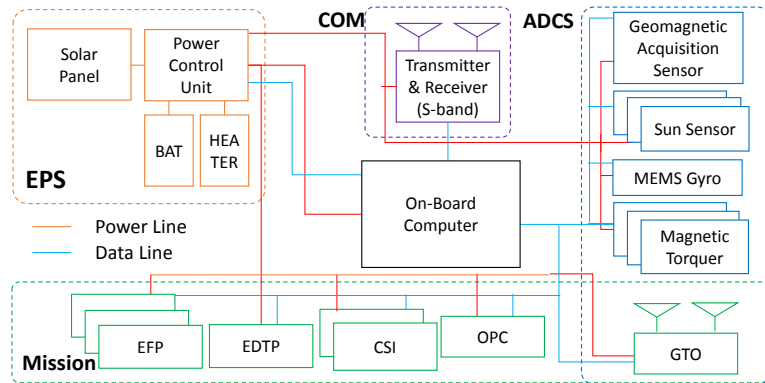


Fig. 7 System dialog

### 5. Space Segment Description

Our satellite configuration is as shown in Fig. 6. Total mass and size of the satellite are 32.1 kg and 12U, which is enough small for a piggyback of a normal launcher such as H-IIA. Taking benefit of the vertical dipole measurements and satisfying mission requirements, gravity gradient stabilization torque helps the attitude stabilization. This configuration also provides not only AC but also DC electric field measurements at high Ne. The glass cover of solar panels is conductive material coated by well-known SnO<sub>2</sub> and at ground to shield the DC potentials on the cells that disturb DC electric field measurements and electric noise from internal satellite subsystems and from solar-panel electronics inducing a large background at ELF and VLF.

From the mission requirements, the satellite needs 1) rough attitude stabilization ( $< 37$  deg.,  $< 1$  rpm) and 2) rough attitude determination ( $< 5$  deg.) for the attitude determination and control system. Therefore, the attitude control system consists of three sun sensors, a geomagnetic sensor, a MEMS gyro and three magnetic torquers. For the communication

Table 2 Telemetry

	Unit	min	max
Transmit EIRP	dBW	-7.13	-1.66
Transmitter Power	W	0.3	0.3
Internal Loss	dB	-3.9	-3.9
Antenna Gain	dBi	2	7.465
Free propagation range	km	2563.15	700.00
Atmospheric absorption loss	dB	-0.00305	-0.0031
Rain fade	dB	-0.08	-0.0056
Receiving G/T	dB/K	7.70	7.70
Antenna Gain	dBi	36.74	36.74
Internal Loss	dB	-2.50	-2.50
System noise temp.	K	450	450
Receiving C/N0	dBHz	61.52	78.33
Required Eb/N0(BER : 10 <sup>-5</sup> )	dB	6	6
Symbol Rate	kbps	64	64
Required C/N0	dBHz	-54.06	-54.06
Hardware loss	dB	-1.5	-1.5
Link Margin	dB	5.96	22.77

capability, 70 MB/day data downlink is needed including the margin. The details of the data amounts are summarized in Fig. 5. Here, we consider the two main ground station, Norway (Svalbard) and Japan. In that case, the total access duration is about 3 hours/day and required data rate becomes 64.2 kbps. Here, the ground stations have 3.8 m parabola antennas with 60% efficiency. The satellite downlink system uses the 0.3 W transmitter with BPSK modulation and the quasi-omnidirectional antenna (a set of two patch antenna). In that case, the link margin becomes larger than 5 dB, as shown in Table 2. Here, the command data rate is set to 4 kbps and the PCM-PSK-PM modulation is decided to be used. With the same antenna set and 10 W ground transmitter, the command line's link margin becomes larger than 20 dB.

Solar cells embedded over upper and 2-side satellite surfaces (5S2P and 5S1P) and deployed two solar panels (5S3P) produces a power balance shown in Fig. 8. Total average consumption of the bus (8 W) and mission (2.8 W) is 10.8 W, which satisfies the power balance on one orbit.

## 6. Orbit/Constellation Description

The mission requires the higher altitude because the visible ground area of the mission equipment becomes wider. However, the OPC has the limit for the altitude because of its resolution requirement. Considering the visible camera resolution limit and its margin, the spacecraft's altitude is decided to be 700 km. From the TEC requirement, the satellite has to put in the sun-synchronous orbit. The mission accept  $\pm 1.5$  hour local time changes and the system does not need propulsion system.

Satellite bus systems are simply designed for the developing countries to easily accomplish the construction. The design concept, therefore, is simple configuration. For example, the complicated redundancy technique is omitted because the number of interface (IF) is reduced. Furthermore, the IF of power and communication lines between components is unified, so that each country can update the system with considering their idea. When other groups develop this CubeSat, sequent CubeSat launches especially for the different local time (e.g. 1230LT, 1430LT) provides outstanding constellation observation such as robust statistical data for EQ and lightning missions and the detailed physical understanding for tsunami and global warming missions.

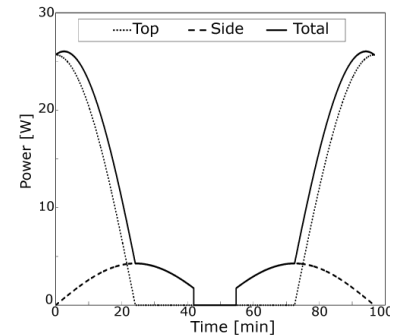


Fig. 8 Power balance on one orbit.

## 7. Implementation Plan

We only employ only matured space-technology for this CubeSat, although some of new ideas are applied. As a piggy-bag launch provided by the space agency such as JAXA without any charge can be applied, the total estimated costs at most 200k US dollars, which enable all of us to find the under a general giant scientific financial support in many country.

## 8. References

- [1] M. Kamogawa et al., Project of Micro-Satellite Constellation for Earthquake Precursor Study, Innovative Ideas for Micro/Nano-satellite Missions, IAA Book Series –Vol. 1 Num. 3, Small Satellites - Programs, Missions, Technologies and Applications, Paris, pp. 16-27 (2013)
- [2] F. Němec et al., Spacecraft observations of electromagnetic perturbations connected with seismic activity, *Geophys. Res. Lett.*, **35**, L05109 (2008).
- [3] S. Togo and M. Kamogawa, Ionospheric earthquake precursors on satellite measurement: physical features and predictability, International workshop earthquake precursor, Taiwan, May 17, Taipei Nangang Exhibition Center, Taiwan (2016).
- [4] Y. Kakinami and M. Kamogawa et al. (2012), Tsunamigenic ionospheric hole, *Geophys. Res. Lett.*, **39**, L00G27 (2012).
- [5] M. Kamogawa et al., A possible space-based tsunami early warning system using observations of the tsunami ionospheric hole (in prep.) (2016)
- [6] D. M. Smith et al., Terrestrial Gamma-Ray Flashes Observed up to 20 MeV, *Science*, **307**, 1085 (2005)
- [7] T. Torii, T. Sugita, M. Kamogawa et al., Migrating source of energetic radiation generated by thunderstorm activity, *Geophys. Res. Lett.*, **38**, L24801, (2011).
- [8] M. Kamogawa et al., Simultaneous Observations of Atmospheric Electric Field, Aerosols, and Clouds on the R/V Hakuho Maru over the Pacific Ocean, *J. Atmos. Electricity*, **34**, 21 (2014)
- [9] E. R. Williams, The Schumann Resonance: A Global Tropical Thermometer, *Science*, **256**, 184 (1992)
- [10] F. Simoes et al., Satellite observations of Schumann resonances in the Earth's ionosphere, *Geophys. Res. Lett.*, **8**, L22101 (2011)
- [11] J.J. Bertheliet et al., ICE, The electric field experiment on DEMETER, *Planetary Space Sci.*, **54**, 456 (2006)
- [12] Y. Kakinami & M. Kamogawa et al., Validation of electron density and temperature observed by DEMETER, *Adv. Space Res.*, **52**, 1267 (2013)
- [13] E. Axell et al., GNSS spoofing detection using multiple mobile COTS receivers, *IEEE Int. Conf. Acous., Speech & Signal Processing*, 3192 (2015)